

SiC Dots in Amorphous-Si and Poly-Si Substrates Fabricated by Hot-C⁺-Ion Implantation

T. Mizuno, R. Kanazawa, Y. Omata, T. Aoki, and T. Sameshima*

Kanagawa Univ., Hiratsuka, Japan (mizuno@info.kanagawa-u.ac.jp), * Tokyo Univ. of Agric. and Tech., Koganei, Japan

Abstract

We experimentally studied SiC nano-dots in an amorphous-Si (a-Si) and poly-Si on quartz substrates fabricated by hot-C⁺-ion implantation technique and post-N₂ annealing, comparing with SiC-dots in a (100) crystal-Si (c-Si) on SOI substrate. We clarified the three Si material structure dependence of photoluminescence (PL) properties of SiC dots. Even in the poor crystal quality substrates of C⁺-ion implanted a-Si and poly-Si layers, we verified 3C-SiC dots by TEM observation, and the strong PL intensity I_{PL} in the near-UV/visible regions. The I_{PL} 's of a-Si and poly-Si after N₂ annealing are much higher than the I_{PL} of c-Si, because a-Si is partially poly-crystallized by high temperature process.

I. Introduction

Using self-cluster effects of C atoms in a hot-C⁺ implanted crystal-Si (c-Si) layer, TEM observation showed that 3C-SiC and hexagonal-SiC (H-SiC) nano-dots (diameter $R \approx 2\text{nm}$) grow into the surface oxide layer from the (100)c-Si surface in both SOI and bulk-Si substrates [1], [2]. We demonstrated the very large bandgap E_G ($\approx 3\text{eV}$) (=peak PL-wavelength λ_{PL} of 400nm) and very strong PL emission I_{PL} in the near-UV/visible regions ($>400\text{nm}$) from the quantum dots of SiC, which is attributable to the electron wave number uncertainty induced PL quantum efficiency increase by strong quantum confinement of electrons in a finite zero-dimensional (0D)-SiC-dot [2]. Thus, the SiC dot technique in Si substrate is very suitable for visible Si-based photonic devices [3]. To clarify the physical mechanism for forming SiC dots in the C⁺ implanted Si layer, as well as to realize practical and low-cost Si-based photonics, it is strongly required to study the Si material structure (such as, amorphous-Si (a-Si), poly-Si, and c-Si) dependence of SiC-dot formation and the PL properties.

In this work, we experimentally studied the SiC dots in an a-Si and poly-Si layers on quartz fabricated by the hot-C⁺-ion implantation and the post-N₂ annealing. We successfully evaluated the material structure and PL property comparison of SiC dots between three Si material structures of a-Si, poly-Si, and c-Si layers.

II. Experiment Procedure

SiC nano-dots were fabricated by the hot-C⁺-ion implantation into three different Si material structures of an a-Si (55-nm thick), poly-Si (20-nm thick) layer on quartz substrates, and (100)c-Si (20-nm thick) on SOI at low (600°C) or high substrate temperature T (800°C) (Fig.1(b)) after sputtering 100-nm-thick surface oxide (SOX) (Fig.1(a)). Post N₂ annealing was carried out at annealing temperature $T_N=1000^\circ\text{C}$ and various annealing time t_N ($0 < t_N \leq 60\text{min}$), to poly-crystallize the a-Si, as well as to recover the C⁺ ion implantation induced damage in Si (Fig.1(c)). C⁺-ion dose D_C was set to be $6 \times 10^{16}\text{cm}^{-2}$, which is an optimum condition for strong I_{PL} [1]. In this work, we formed two samples with ($t_N > 0$ Sample) and without N₂ annealing ($t_N = 0$ Sample). XPS analysis for c-Si at $D_C=4 \times 10^{16}\text{cm}^{-2}$ showed that C atoms are segregated at the SOX/Si interface (25at.%) [2], and thus, it is expected that the maximum C content is higher than 25at.% in these three Si material structures.

PL and Raman properties of SiC dots were measured at room temperatrure, where the excitation laser energy and diameter were 3.8eV and 1μm, respectively. The PL spectrum in the wide range of λ_{PL} from the UV to NIR regions was calibrated using a standard illuminant.

III. Results and Discussions

A. Material Structures of C⁺ Implanted a-Si and poly-Si

Because of random crystal direction of a-Si and poly-Si, it was difficult to find out the SiC dots at SOX/Si interface by CSTEM. However, CSTEM lattice images and electron diffraction (ED) patterns show that 3C-SiC dots were successfully formed in Si layer even in both a-Si and poly-Si layers (Fig. 2), and thus, it is expected that a 3C-SiC and H-SiC dots are formed even at the SOX/Si interface of a-Si and poly-Si, as observed in c-Si [2]. Moreover, Si lattice spots indicate that a-Si was partially poly-crystallized after short N₂ annealing (Fig. 2(a)), which leads to the successful formation of SiC dots even in a-Si. Consequently, we

experimentally confirmed that SiC dots can be formed even in poor crystal quality substrates of a-Si and poly-Si.

Raman analysis (Fig. 3(a)) also shows that a-Si layer at $T=600^\circ\text{C}$ before N₂ annealing is still amorphous, but is poly-crystallized after short N₂ annealing. Moreover, the a-Si at $T=800^\circ\text{C}$ even without N₂ annealing can be also poly-crystallized (Fig. 3(a)), which is the advantageous characteristics of hot-C⁺-implantation. On the other hand, Raman peaks of G and D bands of graphite (Fig. 3(b)) show that implanted C atoms are partially separated out in Si layers, which is reduced by increasing the Si crystal quality.

B. PL Properties of a-Si, poly-Si, and c-Si

We demonstrated the PL emission even from C⁺ implanted a-Si and poly-Si layers (Fig.4), and the maximum I_{PL} ; I_{MAX} of a-Si and poly-Si is higher than I_{MAX} of (100)c-Si (Figs.4 and 5). Moreover, new PL peak at lower PL energy E_{PH} was observed only in a-Si (Fig.4). Thus, the PL spectrum strongly depends on the three Si material structures, which suggests that the SiC dot size and density are affected by the Si material structure.

I_{MAX} strongly depends on t_N , and rapidly increases at $0 < t_N \leq 10\text{min}$ (Fig.5), whereas I_{MAX} is very low before poly-crystallization of a-Si at $t_N=0$. The $I_{MAX}(t_N)$ enhancement factors of a-Si, poly-Si and c-Si, compared with $I_{MAX}(0)$, reach 5.8, 3.9, and 2.6 at $t_N \approx 10\text{min}$, respectively, which is probably attributable to the Si crystal quality improvement after N₂ annealing (Fig.3(a)). However, $I_{MAX}(t_N)$ saturates at $t_N > 30\text{min}$. I_{MAX} of poly-Si is the highest in three Si material structures, and is higher than I_{MAX} of a-Si, which is attributable to the low poly-crystallization rate in a-Si. Lowest I_{MAX} of (100)c-Si is not physically understood at present, but is perhaps due to the Si crystal direction dependence of SiC dot formation.

Measured PL spectra of a-Si and poly-Si can be explained by different SiC-polytype dots of 3C-SiC (I_{3C}), 8H-SiC (I_{8H}), 6H-SiC (I_{6H}), and 4H-SiC (I_{4H}) (Fig.6(a)) at the SOX/Si interface, but PL of a-Si originates from additional one-component I_{SC} with lower E_G , as well as four SiC-polytypes (Fig.6(b)). Hexagonality increases from 0% of 3C-SiC to 50% of 4H-SiC, and the E_G also increases from 2.4eV of 3C-SiC to 3.28eV of 4H-SiC [4]. The I_{SC} of a-Si is perhaps PL emission from nano-dots of Si-C alloy with low C content [5]. Consequently, the measured PL spectrum is the sum of PL emissions from the different material structures, and thus the PL's of a-Si, poly-Si, and c-Si are consisted of different ratio of I_{PL} components; I_{4H} to I_{SC} .

Each peak- I_{PL} components are strongly depends on t_N , too (Figs.7), and have the maximum at $t_N \approx 10\text{min}$ similar to $I_{MAX}(t_N)$ (Fig.5). The ratio of I_{PL} components also depends on the Si material structures of a-Si (Fig.7(a)), poly-Si (Fig.7(b)) and c-Si, which is probably caused by the SiC dot formation difference between three material structures. The ratio of I_{PL} components can be precisely determined by total PL photon count defined by integrated PL intensities of each component; $\int I_{PL}(E_{PH})dE_{PH}$ (Fig.7(c)). In both a-Si and poly-Si, 8H- and 6H-SiC components are the main PL emission. However, in c-Si, the I_{3C} component is relatively high.

The t_N dependence of each peak- E_{PH} of SiC dots is relatively small (Fig.8), and thus the t_N dependence of the SiC dot size R is small, because $E_G \propto R^{-2}$ [4]. Therefore, the N₂ anneal induced I_{PL} enhancement is not caused by the PL quantum efficiency increase with reducing R , but is attributable to the Si quality improvement.

IV. Conclusion

In this work, we experimentally clarified the three Si material structure dependence on SiC dot formation and the PL properties, using the hot-C⁺-ion implantation technique. Even in the poor Si quality of a-Si and poly-Si layers, we demonstrated very strong PL intensity. Thus, hot-C⁺-ion implantation process for a-Si and poly-Si is very promising for low-cost Si-based photonic devices.

Acknowledgement: This work was partially supported by KAKENHI (17K06359).

References: [1] T.Mizuno, Ext. Abst. SSDM, p.597 (2017). [2] T.Mizuno, JJAP **57**, 04FB03 (2018). [3] S. Saito, IEDM 2008, Paper 19.5. [4] J.Fan, *Silicon Carbide Nanostructures* (Springer), 2014. [5] T.Mizuno, JJAP **55**, 04EB02 (2016)

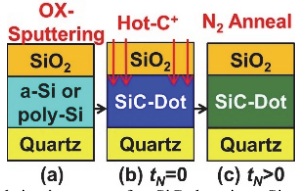


Fig.1 Fabrication steps for SiC dots in a-Si or poly-Si substrates by hot- C^+ -ion-implantation. After (a) sputtering SiO_2 on a-Si or poly-Si substrates, (b) hot- C^+ -ions were implanted at low (600°C) or high T (800°C), where $D_c=6\times 10^{16}\text{cm}^{-2}$ ($t_N=10\text{min}$). (c) N_2 annealing was carried out at $T_N=1000^\circ\text{C}$ ($t_N>0$ Sample).

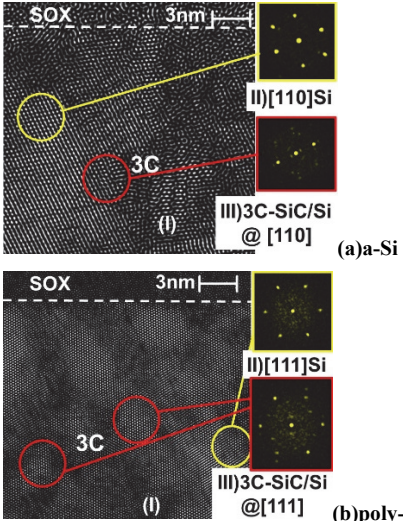


Fig.2 Corrector-spherical aberration TEM (CSTEM) images (I) of cross section of (a) a-Si at $t_N=10\text{min}$ and (b) poly-Si at $t_N=5\text{min}$, and the ED patterns (II)-(III) evaluated by fast Fourier transform (FFT) analysis of the CSTEM data, where $D_c=6\times 10^{16}\text{cm}^{-2}$ and $T=600^\circ\text{C}$. Areas encircled in red of (a) and (b) show the interference patterns of double layers of [110] and [111] 3C-SiC/Si, respectively, which is the direct verification of SiC dots.

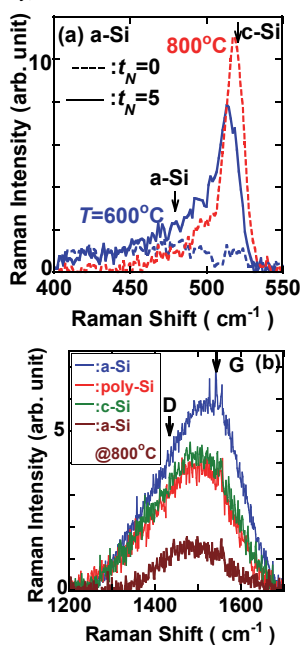


Fig.3 Raman spectra of (a) Si-peak of a-Si, where dashed (blue: $T=600^\circ\text{C}$, red: $T=800^\circ\text{C}$) and solid lines show the data at $t_N=0$ and 5min, respectively. (b) Raman peaks of G/D-bands of a-Si, poly-Si, and c-Si, where $t_N=0$, $T=600^\circ\text{C}$, and 800°C (only a-Si). Arrows in (a) show the Raman peaks of a-Si (480cm^{-1}) and c-Si (520cm^{-1}). Arrows in (b) show the Raman peaks of G and D bands of graphite, respectively.

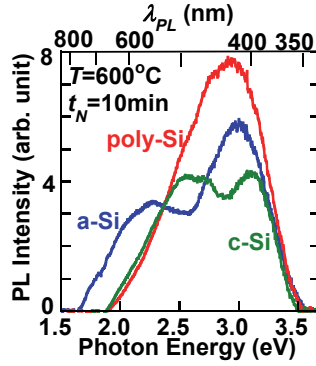


Fig.4 SiC-dot PL spectrum comparison between a-Si (blue), poly-Si (red), and c-Si (green), where $T=600^\circ\text{C}$ and $t_N=10\text{min}$.

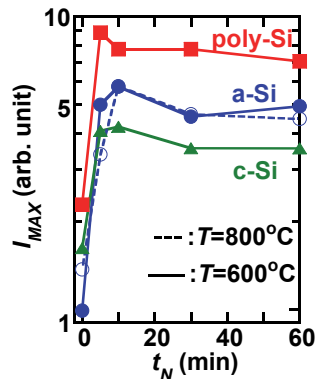


Fig.5 t_N dependence of I_{MAX} of a-Si (circles), poly-Si (squares), and c-Si (triangles) at $T=600^\circ\text{C}$ (solid lines) and 800°C (dashed line).

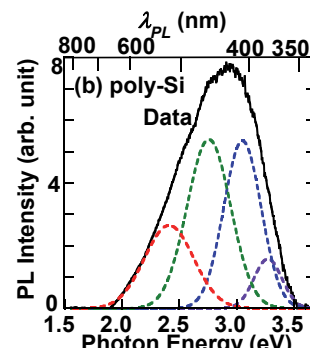
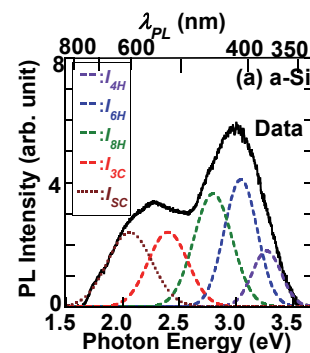


Fig.6 Gaussian curve (dashed lines) fittings for measured PL spectra (solid lines) of (a) a-Si and (b) poly-Si, where $T=600^\circ\text{C}$ and $t_N=10\text{min}$. PL of poly-Si can be explained by four different polytypes of 3C- (I_{3C} : red), 8H- (I_{8H} : green), 6H- (I_{6H} : blue), and 4H-SiC (I_{4H} : purple), but PL of a-Si originates from additional one-component I_{SC} (brown), as well as four SiC-polytypes.

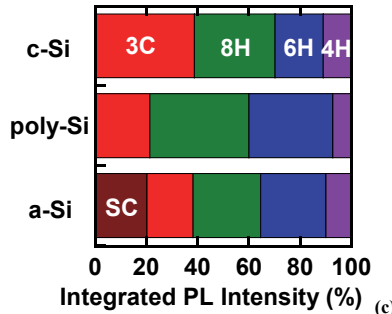
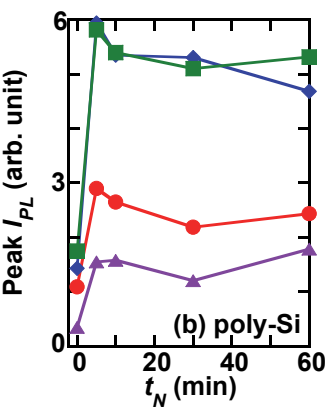
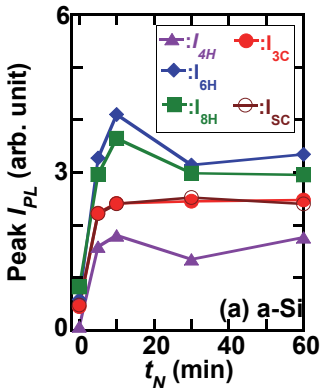


Fig.7 t_N dependence of peak- I_{PL} of each PL component of Figs.6 in (a) a-Si and (b) poly-Si, where $T=600^\circ\text{C}$ and $t_N=10\text{min}$. Triangles, rhombi, squares, circles, and open-circles show I_{4H} , I_{6H} , I_{8H} , I_{3C} , and I_{SC} , respectively. (c) Ratio of integrated PL intensities of each PL component in a-Si, poly-Si, and c-Si, where $T=600^\circ\text{C}$ and $t_N=10\text{min}$.

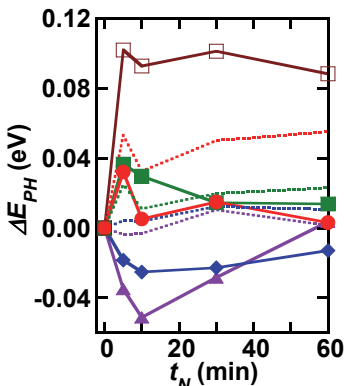


Fig.8 t_N dependence of peak- $E_{PH}(t_N)$ -shift from peak- E_{PH} at $t_N=0$ of each different PL component in a-Si (solid lines) and poly-Si (dashed lines). Triangles, rhombi, squares, circles, and open-circles show the E_G shifts of I_{4H} , I_{6H} , I_{8H} , I_{3C} , and I_{SC} , respectively.